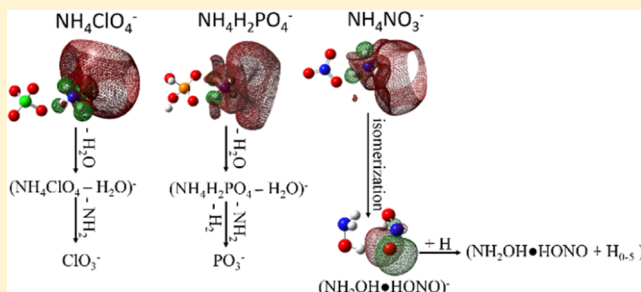# Ammonium Perchlorate and Ammonium Dihydrogen Phosphate as Energetic Materials: Comparison to Ammonium Nitrate

Zhen Zeng and Elliot R. Bernstein*

Department of Chemistry, NSF ERC for Extreme Ultraviolet Science and Technology, Colorado State University, Fort Collins, Colorado 80523, United States

ABSTRACT: Ammonium perchlorate (NH_4ClO_4) and ammonium dihydrogen phosphate $(NH_4H_2PO_4)$ are investigated through laser ablation/matrix-assisted laser desorption ionization processes, anion photoelectron spectroscopy (PES), and density functional theory calculations. No parent anionic species are observed in the mass spectra of these two energetic species. Instead, abundant fragmentation ions for perchlorate are $(NH_4ClO_4-H_2O)^-$ and ClO_3^- and those for dihydrogen phosphate are $(NH_4H_2PO_4-H_2O)^-$ and PO_3^-. Their vertical detachment energies and anionic structures are determined and identified through calculations.

$(NH_4H_2PO_4-H_3O)^-$ is additionally detected through PES. Both $NH_4ClO_4^-$ and $NH_4H_2PO_4^-$ parent anions possess a dipole bound extra electron distributed around the H atoms of the NH_4 group. Based on the calculations, the fragmentation pathway for loss of H_2O from either molecule involves detachment of two hydrogens from NH_4 and one O from ClO_4 or PO_4H_2. These current investigation results are compared to those previously established for NH_4NO_3, which include hydration, addition of H, isomerization, and reactive intermediate formation. The rich anion chemistry found for NH_4NO_3 is thereby further emphasized and characterized. This chemistry may well be responsible for NH_4NO_3's enhanced energetic properties.

1. INTRODUCTION

Ammonium perchlorate (NH_4ClO_4), ammonium dihydrogen phosphate $(NH_4H_2PO_4)$, and ammonium nitrate (NH_4NO_3) are frequently employed as energetic materials for various military and commercial applications. NH_4ClO_4 is widely used as an oxidizing agent for solid rocket propellants in defense activities and the aerospace industry.[1] Its deflagration and thermal decomposition characteristics have been intensively studied:[2–6] the chemical composition of different decomposition products have been investigated.[7–12] Final products derived from NH_4ClO_4 are O_2, N_2, Cl_2, N_2O, NO, NO_2, H_2O, HCl, ClO_2, ClO_3, and NH_3. Electron radiolysis decomposition mechanisms are also explored for ammonium perchlorate: observation of three classes of product molecules suggests that the initial decomposition steps involve generation of ammonia (NH_3) [through a loss of a proton from ammonium ions (NH_4^+)] and formation of chlorate ion ClO_3^- (through decomposition of the perchlorate ion ClO_4^-).[13]

Ammonium dihydrogen phosphate $(NH_4H_2PO_4)$ has broad applications in agricultural fertilizers, nonlinear and integrated optics, and electronics.[14–16] A number of studies of $NH_4H_2PO_4$ have focused on the crystal structure, optical properties, and electrical conductivity.[17–21] Chemical decomposition into phosphoric acid (H_3PO_4) and ammonia (NH_3) is confirmed at a high temperature (153 °C) by means of differential scanning calorimetry, thermogravimetric analysis, and mass spectrometry investigations.[22]

Isolated NH_4ClO_4 and $NH_4H_2PO_4$ (see Figure 1) are explored in the present work through anion photoelectron
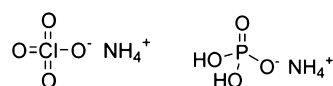

Figure 1. Schematic structures of NH_4ClO_4 (left) and $NH_4H_2PO_4$ (right).

spectroscopic experiments supported by density functional theory (DFT) calculations. The results of the theory and experiments for these two systems are then compared with those previously established[23] for NH_4NO_3 under identical conditions. Gas phase, isolated dissociation ions $(NH_4ClO_4-H_2O)^-$, ClO_3^-, $(NH_4H_2PO_4-H_2O)^-$, and PO_3^- are observed in mass spectra: dissociation pathways through loss of H_2O first from the anionic parent species are suggested (two hydrogens from the NH_4 moiety and one oxygen from Cl/P). Ammonium nitrate does not display these simple dissociation patterns. The release of NH_4NO_3 stored chemical energy evolves through isomerization and formation of hydrogenated cluster anions that can incorporate up to 5 H atoms/NH_4NO_3 molecular species. The unique and distinguishably richer anion chemistry for NH_4NO_3 than for NH_4ClO_4 and $NH_4H_2PO_4$ is thus further confirmed, and may well be the reason for ammonium nitrate's superior behavior as an energetic material.
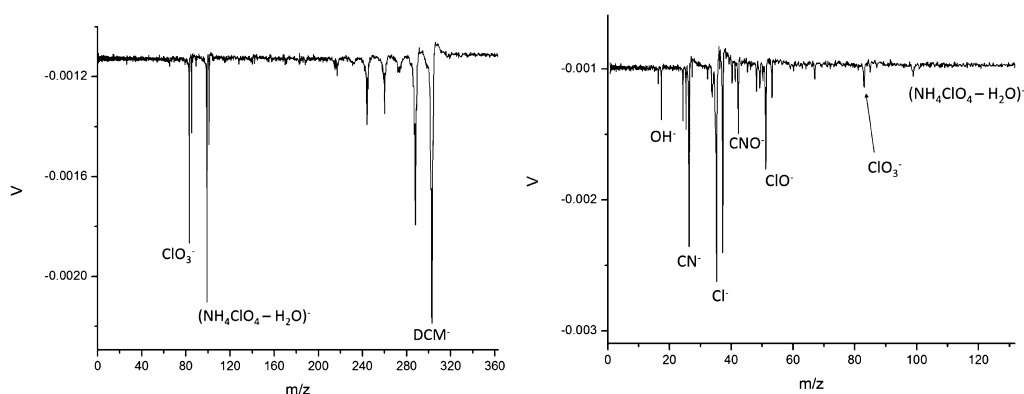
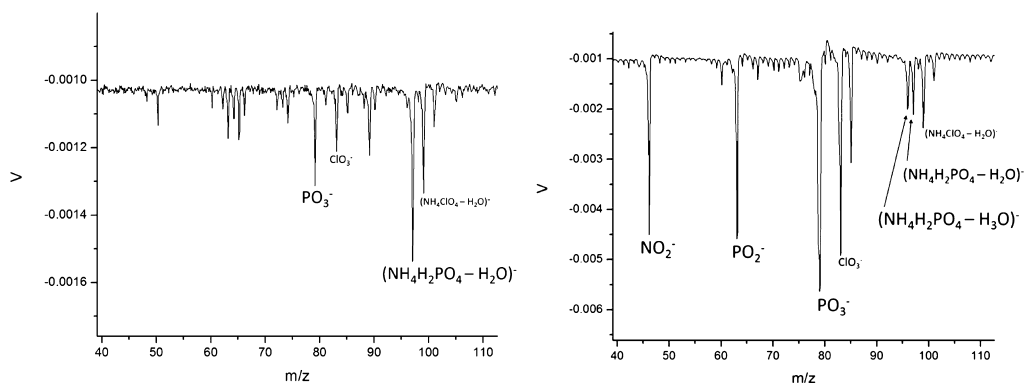**Figure 2.** Mass spectrum of NH_4ClO_4 with the sample (NH_4ClO_4/DCM) spayed on a Zn substrate (left) and the mass spectrum of NH_4ClO_4 through direct laser ablation of the pure sample (right). Laser wavelength is 532 nm (2.331 eV).

Figure 3. Mass spectrum of $NH_4H_2PO_4$ with the sample ($NH_4H_2PO_4$/DCM) spayed on a Zn substrate (left) and the mass spectrum of $NH_4H_2PO_4$ through direct laser ablation of the pure sample (right). Mass peaks from contamination of NH_4ClO_4 in the $NH_4H_2PO_4$ sample are observed. Laser wavelength is 532 nm (2.331 eV).

2. EXPERIMENTAL PROCEDURES

The experimental apparatus consists of three parts: a pulsed supersonic nozzle with an attached matrix assisted laser desorption ionization (MALDI) source, a reflectron time of a flight mass spectrometer (RTOFMS), and a magnetic bottle photoelectron TOF spectrometer (MBTOFPES). Details of this system (RTOFMS/MBTOFPES) can be found in our previous publications.[24,25] The nozzle employed for the sample beam generation is constructed from a Jordan Co. pulsed valve with a homemade laser desorption attachment. Sample drums for the MALDI process are prepared by wrapping the sample desorption substrate Zn on a clean Al drum.[26] A mixed solution of ammonium salt and matrix dichloromethane (DCM) dye with a mole ratio ~1:2 in a solvent (typically, acetonitrile and water) is uniformly sprayed on the drum/substrate surface using an air atomizing spray nozzle (Spraying System Co.) with a siphon pressure of 10 psig. During the spraying process, the sample drum is rotated under heat of a halogen lamp (<70 °C) in a fume hood to ensure deposition of ammonium perchlorate/ammonium dihydrogen phosphate and matrix on the drum surface is homogeneous and dry. The well coated and dried sample drum is then placed in the laser ablation head/nozzle assembly and put into the vacuum chamber. Second harmonic (532 nm) light pulses from a Nd:YAG laser are used to ablate the sample drum, which rotates and translates simultaneously to maintain a fresh sample area for each laser ablation pulse. Whole ammonium salt molecules are desorbed from the drum, interact with other species (including electrons) in the ablated material plume, are entrained in the supersonic flow of the helium carrier gas with a 50 psi backing pressure through a 2 × 60 mm channel in the ablation head, and expanded into the sample chamber. For directly ablating pure ammonium salt samples with no dye present, the dried pure ammonium salt sample drum is made by spraying a pure ammonium salt/water solution and evaporating the water as above. With a closed pulsed valve, the RTOFMS chamber pressure is ~6 × 10^{-8} Torr. The generated molecular anions are pulsed into the RTOFMS and are mass analyzed using the RTOFMS. For photoelectron spectroscopy (PES) experiments, specific anions are first mass selected and decelerated before interacting with a 355 nm (3.496 eV) or 266 nm (4.661 eV) laser beam from another Nd:YAG laser in the photodetachment region. Photodetached electrons are collected and energy analyzed by the MBTOFPES at nearly 100% efficiency. The photodetachment laser is operated at a 10 Hz repetition rate, while the ablation laser is synchronously triggered at 5 Hz. Data are collected at 5 Hz employing a background subtraction with alternation of the ablation laser on/off if the detachment laser wavelength is equal to or less than 266 nm. Every photoelectron spectrum is calibrated by the known spectra of Cu$^-$ at the employed detachment photon energy. The photoelectron energy resolution is ~4% (40 meV for 1 eV kinetic energy electrons), as anticipated for a 1 m PES flight tube.

3. COMPUTATIONAL METHODS

The geometry optimizations are conducted based on DFT with a ωB97XD functional[27] and Dunning's correlation

consistent with the aug-cc-pvtz basis set for all atoms, as executed in the Gaussian 09 program.[28] The ωB97XD functional is evaluated to be able to predict electronic and geometric structures accurately for noncovalently bonded interacting systems. This DFT level has been tested successfully on the NH_4NO_3 system and demonstrated to be sufficient for analysis of the results of NH_4NO_3 observed chemistry.[23] No symmetry restrictions are applied throughout the calculations. Harmonic vibrational frequencies are calculated during optimization to confirm that the obtained structures are the true local minima. Theoretical VDEs for each anionic species are calculated as the energy difference between the ground state of the anion and its corresponding neutral at the same structure as the anion. Natural bond orbital (NBO) analysis is performed based on the ωB97XD/aug-cc-pvtz level of theory for further electronic structure based understanding of parent and fragment anionic species behavior.

4. EXPERIMENTAL RESULTS

Through MALDI generation processes, the mass spectrum of NH_4ClO_4 presents major detected anion species $(NH_4ClO_4-H_2O)^-$ and ClO_3^- $((NH_4ClO_4-H_2O-NH_2)^-)$, as shown in Figure 2 (left). No parent anion $NH_4ClO_4^-$ RTOFMS feature is observed. Additional fragmentation anions, such as ClO^-, Cl^-, and OH^-, are accessed through direct laser ablation of the pure sample, as can be seen from Figure 2 (right).

Similarly, fragmentation anions $(NH_4H_2PO_4-H_2O)^-$ and PO_3^- $((NH_4H_2PO_4-H_2O-NH_2-H_2)^-)$ are predominantly accessible in the mass spectrum of $NH_4H_2PO_4$ generated by the MALDI method (Figure 3); further dissociation anions PO_3^-, PO_2^-, and NO_2^- are observed through direct laser ablation of the sample surface. No parent anion $NH_4H_2PO_4^-$ is observed by either method of sample generation. Another mass feature $(NH_4H_2PO_4-H_3O)^-$ surprisingly appears for the directly ablated sample. Using 266 nm photons, no PES features can be detected for $(NH_4ClO_4-H_2O)^-$, ClO_3^-, $(NH_4H_2PO_4-H_2O)^-$, and PO_3^-. The photoelectron spectrum of $(NH_4H_2PO_4-H_3O)^-$ is recorded and mainly shows two features, one centered at 1.18 eV and another centered at ~2.75 eV, as shown in Figure 4. A weak tail of this latter feature is cut off by photon energy (4.661 eV) for 266 nm laser light generated PES.

5. THEORETICAL RESULTS AND DISCUSSION

The low energy isomers of $NH_4ClO_4^-$, $(NH_4ClO_4-H_2O)^-$, ClO_3^-, $NH_4H_2PO_4^-$, $(NH_4H_2PO_4-H_2O)^-$, $(NH_4H_2PO_4-H_3O)^-$, and PO_3^- are optimized via a ωB97XD/aug-cc-pvtz DFT approach, summarized from Figures 5−7.

The optimized geometries of parent anions $NH_4ClO_4^-$ and $NH_4H_2PO_4^-$ are shown to have small calculated VDEs of 0.70 and 0.22, respectively, as reported in Figure 5. The highest singly occupied molecular orbitals (HSOMOs) of these two parent anions generated from an NBO analysis exhibit diffuse dipole-bound electron orbitals around H atoms of the NH_4 unit. $NH_4ClO_4^-$ and $NH_4H_2PO_4^-$ are significantly unstable in this anionic form, which can explain their absence in the experimental data: they can subsequently undergo fragmentation through loss of H_2O and further dissociation. Observation of the fragmentation ions, $(NH_4ClO_4-H_2O)^-$ and $(NH_4H_2PO_4-H_2O)^-$, as well as small dissociation ions $(ClO_3^-, PO_3^-, ClO^-, NO_2^-, ...)$ also illustrates that the
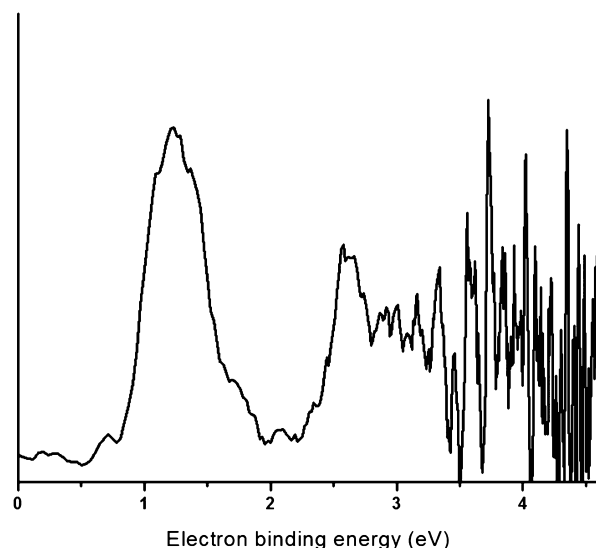
Figure 4. Photoelectron spectrum of $(NH_4H_2PO_4-H_3O)^-$. Laser wavelength is 266 nm (4.661 eV).

$NH_4ClO_4^-$ $NH_4H_2PO_4^-$

VDE: 0.70 eV   VDE: 0.22 eV

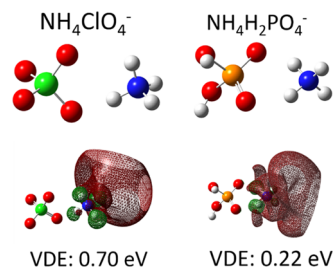**Figure 5.** Optimized geometries and NBO/highest occupied molecular orbitals for $NH_4ClO_4^-$ and $NH_4H_2PO_4^-$ parent anions based on ωB97XD/aug-cc-pvtz calculations. They mostly display a dipole bound character with the added electron distributing around H atoms of the ammonium unit. The calculated VDE are indicated. (O: red, Cl: green, P: orange, N: blue, H: white).
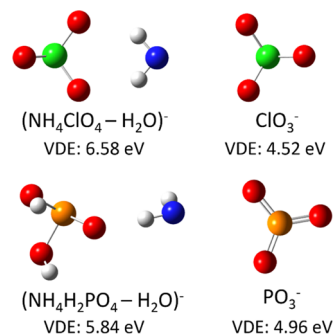

$(NH_4ClO_4 - H_2O)^-$ ClO_3^-
VDE: 6.58 eV   VDE: 4.52 eV

$(NH_4H_2PO_4 - H_2O)^-$ PO_3^-
VDE: 5.84 eV   VDE: 4.96 eV

Figure 6. Optimized geometries for anionic isomers of $(NH_4ClO_4-H_2O)^-$, ClO_3^-, $(NH_4H_2PO_4-H_2O)^-$, and PO_3^- based on ωB97XD/aug-cc-pvtz calculations. The calculated VDEs are indicated. (O: red, Cl: green, P: orange, N: blue, H: white).

anionic structural forms for $NH_4ClO_4^-$ and $NH_4H_2PO_4^-$ are not stable in isolation.

$NH_4ClO_4^-$ and $NH_4H_2PO_4^-$ anions can undergo identical dissociation pathways: they both lose one H_2O unit first and continue to dissociate the NH_2 group or $NH_2 + H_2$ to form a stable anion ClO_3^- or PO_3^-. From Figure 6, both $(NH_4ClO_4-H_2O)^-$ and $(NH_4H_2PO_4-H_2O)^-$ anions have optimized structures showing an NH_2 unit interacting with $ClO_3/$

C

ΔE: 0.00 eV   ΔE: 0.39 eV   ΔE: 4.46 eV
VDE: 4.63 eV   VDE: 5.34 eV   VDE: 2.80 eV
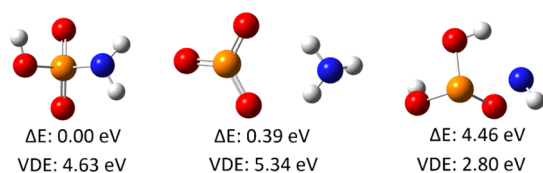
Figure 7. Optimized geometries for anionic isomers of $(NH_4H_2PO_4-H_3O)^-$ based on ωB97XD/aug-cc-pvtz calculations. The calculated VDEs and relative energies are indicated. (O: red, P: orange, N: blue, H: white).

PO$_3$H$_2$ moieties through hydrogen bonding. Their theoretical VDEs are calculated to be 6.58 and 5.84 eV, respectively, which are significantly higher than the 266 nm photon energy. The structure with hydrogen abstraction from the NH$_4$ group and one of the OH groups on H$_2$PO$_4$ (PO$_3$H·NH$_3$) has a lower energy than the isomer (PO$_3$H$_2$·NH$_2$), shown in the Figure 6, by 1.5 eV. It has a calculated VDE of 2.73 eV, not seen from the PES spectrum of $(NH_4H_2PO_4-H_2O)^-$ recorded via 266 nm. The structure PO$_3$H·NH$_3$ can be excluded directly from the experiments. Therefore, we do not show the structure PO$_3$H·NH$_3$ in Figure 6. $(NH_4ClO_4-H_2O)^-$ and $(NH_4H_2PO_4-H_2O)^-$ anions have high VDEs, while the parent anions $NH_4ClO_4^-$ and $NH_4H_2PO_4^-$ evidence low electron binding energies (EBEs). This suggests that the energy difference between the fragment and parent species for anions is greater than that for neutrals. One can further suggest that the extra electron stabilizes the fragmentation species. The structural similarity between $(NH_4ClO_4-H_2O)^-$ and $(NH_4H_2PO_4-H_2O)^-$ suggests identical chemical behavior for NH_4ClO_4 and $NH_4H_2PO_4$. $(NH_4ClO_4-H_2O)^-$ and $(NH_4H_2PO_4-H_2O)^-$ continue to detach NH$_2$/NH$_2$ + H$_2$ to form ClO$_3^-$ and PO$_3^-$, respectively. The calculated VDEs for ClO$_3^-$ and PO$_3^-$ are 4.52 and 4.93 eV, in good agreement with the reported experimental VDEs of 4.65[29] and 4.95[30] eV, respectively.

Three low lying isomers of $(NH_4H_2PO_4-H_3O)^-$ are shown in Figure 7. The lowest energy isomer loses H$_2$ from the NH$_4$ unit and another H from the POH$_2$ moiety, and the remaining NH$_2$ is bound to the P atom. The calculated VDE for the lowest energy isomer of $(NH_4H_2PO_4-H_3O)^-$ is 4.63 eV, which may contribute to the tail of the PE spectrum presented in Figure 4 for $(NH_4H_2PO_4-H_3O)^-$. The second low lying isomer has the NH$_3$ unit interacting with the PO$_3$ moiety through hydrogen bonding. This isomer has a theoretically calculated VDE higher than 266 nm photon energy. The third low lying isomer undergoes 3 H losses from the NH$_4$ unit and evidences weak interaction between remaining NH and one O atom from the PO$_3$H$_2$ moiety. This latter isomer has a calculated VDE of 2.80 eV, which can be assigned to contribute to the higher EBE feature in the PE spectrum of $(NH_4H_2PO_4-H_3O)^-$ given in Figure 4. This isomer is likely to be present in the experiments even at such high relative energy associated with ion generation processes. These generation processes could overcome the respective local energy barriers because of the big structural differences between the calculated local minima. These isomer species can be formed and trapped as different local isomers. Another PES feature (1.18 eV) may be associated with some unknown contamination of the sample, as the calculations do not produce such a low EBE for the $(NH_4H_2PO_4-H_3O)^-$ fragment.

6. CONCLUSIONS

6.1. NH$_4$ClO$_4$ and NH$_4$H$_2$PO$_4$. Ammonium perchlorate (NH$_4$ClO$_4$) and ammonium dihydrogen phosphate (NH$_4$H$_2$PO$_4$), generated as the isolated gas phase species, through both the MALDI and direct ablation methods, are investigated employing TOFMS, anion PES, and DFT calculations. The parent anionic species for NH$_4$ClO$_4$ and NH$_4$H$_2$PO$_4$ are not observed in the mass spectra by the sample generation technique. Fragment ions $(NH_4ClO_4-H_2O)^-$ and ClO$_3^-$ are the major accessible species from NH$_4$ClO$_4$ employing the MALDI approach. Additional dissociation ions, such as ClO$^-$, Cl$^-$, or OH$^-$, are only observed in the mass spectrum through direct laser ablation. Similarly, the dissociation anions $(NH_4H_2PO_4-H_2O)^-$ and PO$_3^-$ from NH$_4$H$_2$PO$_4$ can be accessed in the mass spectrum with DCM present; further fragment ions, such as PO$_2^-$, NO$_2^-$, and $(NH_4H_2PO_4-H_3O)^-$ are observed by TOFMS through direct laser ablation of the pure sample. Clearly the MALDI source, with an absorbing dye matrix, provides a gentler method for the generation of a target species than the direct ablation of the pure sample.

From an NBO/HSOMO analysis, both NH$_4$ClO$_4^-$ and NH$_4$H$_2$PO$_4^-$ parent anions possess a dipole bound extra electron distributed around the H atoms of the NH$_4$ group. Such a structure is unstable and can readily fragment. This explains why parent anionic species are not observed.

PES peaks for $(NH_4ClO_4-H_2O)^-$, ClO$_3^-$, $(NH_4H_2PO_4-H_2O)^-$, and PO$_3^-$ are not detectable employing 266 nm photons. The optimized isomers of $(NH_4ClO_4-H_2O)^-$, ClO$_3^-$, $(NH_4H_2PO_4-H_2O)^-$, and PO$_3^-$ all evidence higher calculated VDEs than the 266 nm photon energy. The identified isomeric structures of $(NH_4H_2PO_4-H_3O)^-$ can evolve from a parent species by losing three H atoms from the NH$_4$ group and one O atom from the phosphate group.

These fragment pattern results give insight into the dissociation process for NH$_4$ClO$_4$ and NH$_4$H$_2$PO$_4$: the NH$_4$ClO$_4^-$ and NH$_4$H$_2$PO$_4^-$ parent anions can lose an H$_2$O unit first, then continue secondary dissociation to form stable anions ClO$_3^-$ and PO$_3^-$.

6.2. Comparison to NH$_4$NO$_3$. Gathered under nearly identical experimental conditions and techniques, the results for NH$_4$ClO$_4$, NH$_4$H$_2$PO$_4$, and NH$_4$NO$_3$[23] can be explored and contrasted. All three parent ammonium salt anions have their dipole bound extra electrons distributed on the NH$_4$ group for the formula geometries and are thereby absent in the observed samples. The observed NH$_4$NO$_3$ anion presents a different, isomerized, detectable parent anion with a stable form $(NH_2OH·HONO)^-$: hydrogenated clusters anions, with up to 5 additional H atoms, are built only on the accessible form $(NH_2OH·HONO)^-$. The other two energetic salts, NH$_4$ClO$_4$ and NH$_4$H$_2$PO$_4$, show only H$_2$O loss dissociation patterns, which have not been identified for NH$_4$NO$_3$. Significant fragmentations to stable anions ClO$_3^-$, PO$_3^-$, and NO$_3^-$ are additionally observed, respectively, for these anionic salts.

The unique and rather surprising chemistry found for NH$_4$NO$_3$ but not NH$_4$ClO$_4$ and NH$_4$H$_2$PO$_4$ presents reactive intermediate formation, as well as isomerization behavior available only to NH$_4$NO$_3$. This richer anion chemistry identified for NH$_4$NO$_3$ is quite possibly the reason for ammonium nitrate's unique importance as an energetic material and an essential fuel component.

■ AUTHOR INFORMATION

Corresponding Author

*E-mail: erb@colostate.edu.

ORCID

Elliot R. Bernstein: 0000-0003-0045-7193

Notes

The authors declare no competing financial interest.

■ REFERENCES

(1) Mattie, D. R.; Strawson, J.; Zhao, J. Perchlorate Toxicity and Risk Assessment. In *Perchlorate: Environmental Occurrence, Interactions and Treatment*; Gu, B., Coates, J. D., Eds.; Springer US: Boston, MA, 2006; pp 169−196.

(2) Khairetdinov, E. F.; Boldyrev, V. V. The mechanism of the low-temperature decomposition of NH4ClO4. *Thermochim. Acta* **1980**, *41*, 63−86.

(3) Boldyrev, V. V. Thermal decomposition of ammonium perchlorate. *Thermochim. Acta* **2006**, *443*, 1−36.

(4) Boldyrev, V. V.; Alexandrov, V. V.; Boldyreva, A. V.; Gritsan, V. I.; Karpenko, Y. Y.; Korobeinitchev, O. P.; Panfilov, V. N.; Khairetdinov, E. F. On the mechanism of the thermal decomposition of ammonium perchlorate. *Combust. Flame* **1970**, *15*, 71−77.

(5) Vyazovkin, S.; Wight, C. A. Kinetics of thermal decomposition of cubic ammonium perchlorate. *Chem. Mater.* **1999**, *11*, 3386−3393.

(6) Hedman, T. D.; Gross, M. L. On the thermal stability of partially decomposed ammonium perchlorate. *Propellants, Explos., Pyrotech.* **2016**, *41*, 254−259.

(7) Bircumshaw, L. L.; Newman, B. H.; Melville, H. W. The thermal decomposition of ammonium perchlorate - I. Introduction, experimental, analysis of gaseous products, and thermal decomposition experiments. *Proc. R. Soc. London, Ser. A* **1954**, *227*, 115−132.

(8) Rosser, W. A.; Inami, S. H.; Wise, H. Thermal decomposition of ammonium perchlorate. *Combust. Flame* **1968**, *12*, 427−435.

(9) Goshgarian, B. B.; Walton, T. A. Mass-spectrometric study of ammonium perchlorate decomposition. *US Air Force Rocket Propulsion Laboratory Technical Report*, 1965; pp 65−87.

(10) Heath, G. A.; Majer, J. R. Mass spectrometric study of the thermal decomposition of ammonium perchlorate. *Trans. Faraday Soc.* **1964**, *60*, 1783−1791.

(11) Leu, A.-L.; Yeh, T.-F. The thermal behaviour of porous residual ammonium perchlorate. *Thermochim. Acta* **1991**, *186*, 53−61.

(12) Góbi, S.; Zhao, L.; Xu, B.; Ablikim, U.; Ahmed, M.; Kaiser, R. I. A vacuum ultraviolet photoionization study on the thermal decomposition of ammonium perchlorate. *Chem. Phys. Lett.* **2018**, *691*, 250−257.

(13) Góbi, S.; Bergantini, A.; Turner, A. M.; Kaiser, R. I. Electron radiolysis of ammonium perchlorate: a reflectron time-of-flight mass spectrometric study. *J. Phys. Chem. A* **2017**, *121*, 3879−3890.

(14) Voronov, A. P.; Salo, V. I.; Puzikov, V. M.; Tkachenko, V. F.; Vydaĭ, Y. T. Potassium and ammonium dihydrogen phosphates activated with thallium: Growth and luminescence and scintillation properties. *Crystallogr. Rep.* **2006**, *51*, 696−701.

(15) Rashkovich, L. N. *KDP-Family Single Crystals*; Hilger: Bristol, 1991.

(16) Rath, J. K.; Radhakrishna, S. Electrical conductivity and dielectric loss studies of MoO4²⁻-doped NH4H2PO4 single crystals. *J. Mater. Sci. Lett.* **1987**, *6*, 929−931.

(17) Ramteke, S. P.; Anis, M.; Baig, M. I.; Shkir, M.; Ganesh, V.; Muley, G. G. Eye-catching modification in external morphology, photoluminescence and SHG efficiency of NH4H2PO4 crystal: A consequence of influential presence of tartaric acid. *Optik* **2018**, *158*, 634−638.

(18) Anis, M.; Hussaini, S. S.; Shkir, M.; AlFaify, S.; Baig, M. I.; Muley, G. G. Uncovering the influence of Ni²⁺ on optical and dielectric properties of NH4H2PO4 (ADP) crystal. *Optik* **2018**, *157*, 592−596.

(19) Shaikh, R. N.; Anis, M.; Shirsat, M. D.; Hussaini, S. S. Systematic analysis on linear and nonlinear optical traits of citrulline doped NH4H2PO4 (ADP) crystal. *Optik* **2018**, *154*, 435−440.

(20) Zhou, H.; Wang, F.; Xu, M.; Liu, B.; Liu, F.; Zhang, L.; Xu, X.; Sun, X.; Wang, Z. Raman spectral characterization of NH4H2PO4 single crystals: Effect of pH on microstructure. *J. Cryst. Growth* **2016**, *450*, 6−13.

(21) Sun, C.; Xue, D. In situ IR spectral observation of NH4H2PO4 crystallization: Structural identification of nucleation and crystal growth. *J. Phys. Chem. C* **2013**, *117*, 19146−19153.

(22) Pardo, A.; Romero, J.; Ortiz, E. High-temperature behaviour of ammonium dihydrogen phosphate. *J. Phys.: Conf. Ser.* **2017**, *935*, 012050.

(23) Zeng, Z.; Bernstein, E. R. Isomeric structures of isolated ammonium nitrate and its hydrogenated species identified through PES experiments and DFT calculations. *Phys. Chem. Chem. Phys.* **2018**, *20*, 11224−11236.

(24) Im, H.-S.; Bernstein, E. R. On the initial steps in the decomposition of energetic materials from excited electronic states. *J. Chem. Phys.* **2000**, *113*, 7911−7918.

(25) Yin, S.; Bernstein, E. R. Properties of iron sulfide, hydrosulfide, and mixed sulfide/hydrosulfide cluster anions through photoelectron spectroscopy and density functional theory calculations. *J. Chem. Phys.* **2016**, *145*, 154302.

(26) Yuan, B.; Yu, Z.; Bernstein, E. R. Initial mechanisms for the decomposition of electronically excited energetic materials: 1,5′-BT, 5,5′-BT, and AzTT. *J. Chem. Phys.* **2015**, *142*, 124315.

(27) Chai, J.-D.; Head-Gordon, M. Long-range corrected hybrid density functionals with damped atom-atom dispersion corrections. *Phys. Chem. Chem. Phys.* **2008**, *10*, 6615−6620.

(28) Frisch, M. J.; Trucks, G. W.; Schlegel, H. B.; Scuseria, G. E.; Robb, M. A.; Cheeseman, J. R.; Scalmani, G.; Barone, V.; Mennucci, B.; Petersson, G. A., et al. *Gaussian 09*, Revision A.02; Gaussian, Inc.: Wallingford CT, 2009.

(29) Wang, X.-B.; Wang, L.-S. The electronic structure and electron affinities of higher chlorine oxide radicals ClOₓ (x=2−4) from photoelectron spectroscopy of ClOₓ⁻ anions. *J. Chem. Phys.* **2000**, *113*, 10928−10933.

(30) Wang, X.-B.; Wang, L.-S. Vibrationally resolved photoelectron spectroscopy of PO3⁻ and the electronic structure of PO3. *Chem. Phys. Lett.* **1999**, *313*, 179−183.